

HyperPose: Camera Pose Localization using Attention Hypernetworks

Ron Ferens, Yosi Keller*
Bar Ilan University

Abstract

In this study, we propose the use of attention hypernetworks in camera pose localization. The dynamic nature of natural scenes, including changes in environment, perspective, and lighting, creates an inherent domain gap between the training and test sets that limits the accuracy of contemporary localization networks. To overcome this issue, we suggest a camera pose regressor that integrates a hypernetwork. During inference, the hypernetwork generates adaptive weights for the localization regression heads based on the input image, effectively reducing the domain gap. We also suggest the use of a Transformer-Encoder as the hypernetwork, instead of the common multilayer perceptron, to derive an attention hypernetwork. The proposed approach achieves superior results compared to state-of-the-art methods on contemporary datasets. To the best of our knowledge, this is the first instance of using hypernetworks in camera pose regression, as well as using Transformer-Encoders as hypernetworks. We make our code publicly available¹.

1 Introduction

In numerous computer vision applications such as indoor navigation, augmented reality, and autonomous driving, it is essential to determine the position and orientation of a camera using a query image. Current camera localization techniques show various trade-offs between accuracy, runtime, and memory usage. The most precise methods [2, 3, 28, 35, 27] involve hierarchical localization

pipelines, which commonly use a coarse-to-fine processing flow that begins with image retrieval to perform an initial localization based on images similar to the query image, followed by local feature extraction and matching. To estimate the camera’s 6-Degrees-Of-Freedom (6DoF) accurately, the resulting 2D-2D matches are mapped to 3D correspondences in the scene’s point cloud and then used to determine the camera pose through Perspective-n-Point (PnP) and RANSAC. Another approach, absolute pose regressors (APRs), can estimate the camera pose with a single forward pass using only the query image, resulting in significantly lower latency, although being notably less accurate. Additionally, due to their low memory footprint, APRs can be deployed as a standalone application on edge devices with limited computational resources. For a survey of visual camera pose localization, refer to [44, 30].

PoseNet by Kendall et al. [17] was the first APR approach, using a convolutional backbone and a multilayer perceptron (MLP) head to regress the camera’s position and orientation. This approach was simple and able to run at 5ms leading to a multitude of APR methods that improve accuracy by modifying the backbone and MLP architectures [21, 22, 40, 42, 31, 41, 6] as well as alternative loss functions and optimization strategies [15, 16, 30]. Indoor and outdoor environments present dynamic scenarios characterized by varying lighting conditions, viewing angles, and moving objects. Thus, fitting a single, global set of parameters to these changing circumstances might limit the network’s adaptability and result in reduced accuracy.

Hypernetworks [14] are a deep learning architecture where an auxiliary network, the hypernetwork, generates the weights for the primary network (main network) based

*yosi.keller@gmail.com

¹<https://anonymus.4open.science/r/hyperpose-2023/>

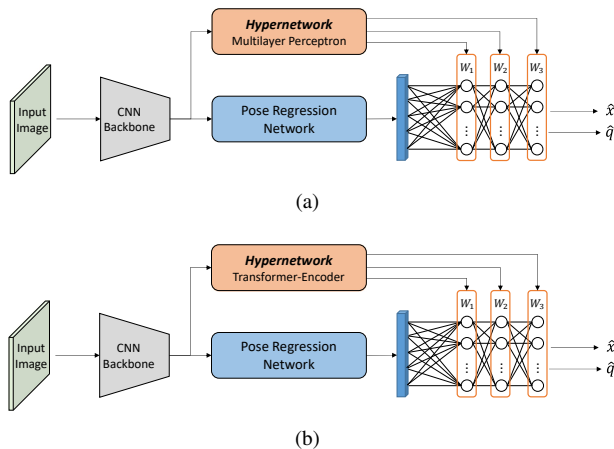


Figure 1: Camera pose localization using hypernetworks. (a) A hypernetwork consisting of a multilayer perceptron computing the weights of the regression head. (b) The regression weights are computed by an attention-hypernetwork consisting of a Transformer-Encoder.

on the current input and the downstream task. The hypernetwork allows for dynamic and adaptive weight modulation of the main network, leading to improved flexibility in response to changing conditions [23, 9]. Both the main network and the hypernetwork are trained in a unified, end-to-end manner through the use of backpropagation-based optimization.

Our approach differs from traditional Absolute Pose Regression (APR) methods that rely on a single global image encoding for estimating the 6DoF pose of a camera [17, 15, 40, 31, 6, 32]. Instead, we use a dual attention-based approach that simultaneously regresses both translation and orientation, providing an adaptive analysis of image content. The spatial content of images contains both informative and uninformative cues, that are effectively handled by our approach. Furthermore, we introduce a novel attention hypernetwork formulation that utilizes Transformer-Encoders as hypernetworks to output coefficients for regression heads based on the input query image. Specifically, the camera pose regression is divided into two separate sequence-to-one problems. Intermediate activation maps are processed by two separate Transformer-Encoders for translation and rotation, as illustrated in Figure 2. The activation maps are also fed into

the relevant attention hypernetwork, which computes the weights for the localization and orientation heads. These predicted weights, combined with the output from the encoders, allow us to perform the regression of the corresponding localization attributes. This approach allows for an adaptive analysis of the image content, enabling the regression weights to focus on informative features for each attribute, rather than relying on a single global image representation. The use of Transformer-Encoders as hypernetworks is a novel formulation that provides improved performance in the regression tasks, compared to traditional fully-connected layers or other neural network architectures. The proposed dual attention-based architecture results in a more robust and accurate model for camera pose regression.

In summary, our research offers three key contributions:

- An absolute pose regression approach using hypernetworks that is experimentally shown to adapt to varying appearance and lighting conditions.
- We propose to use a Transformer-Encoder, instead of the common MLP, as an attention hypernetwork to learn the regression head parameters.
- The proposed scheme achieves new state-of-the-art APR accuracy across outdoor and indoor localization benchmarks.

2 Related Work

2.1 Camera Pose

Camera pose estimation techniques differ by their input during inference and algorithmic attributes.

3D-based or structure-based localization methods are considered to be the most accurate for camera pose estimation and have demonstrated state-of-the-art performance on leading benchmarks. These methods utilize correspondences between 2D features in an image and 3D world coordinates. A two-phase approach was introduced by [12, 27, 24, 25] for hierarchical pose estimation pipelines. In this process, each query image is first encoded using a CNN trained for image retrieval (IR), based

on a pre-mapped image dataset. Tentative correspondences are then estimated by matching local image features to 3D matches. The resulting matches are then used by PnP-RANSAC to estimate the camera pose. DSAC [2] and its follow-up scheme, DSAC++ [3], utilize a CNN architecture to directly estimate the 3D coordinates from 2D positions in an image and only require the query image during inference. The same as in Absolute Pose Regression (APR) methods, separate models must be trained for each scene, achieving state-of-the-art accuracy.

Relative Pose Regression (RPR) algorithms estimate the relative pose between an input query image and a set of reference images based on their known location. Calculating the relative pose involves the estimation of the relative position and orientation between the query image and the reference images [47, 4]. An Image Retrieval (IR) approach is utilized to determine the closest set of neighbor images, and the relative motion is then estimated between the query image and each of the retrieved images. The estimated relative poses are utilized, along with the known position of the reference images, to estimate the camera’s absolute pose. Similarly to 3D and structured-based localization methods, RPRs involve a multistep process and require access to a database of images with labeled poses during the inference phase.

Absolute Pose Regression (APR) directly estimate the camera pose given the input query image. APRs were first introduced by Kendall [17], using a modified version of the truncated GoogLeNet architecture, where the Softmax classification layer was replaced with a series of fully connected layers that output the pose estimate. Although such approaches are less accurate than classical structure-based techniques, they offer several advantages, such as faster inference times (milliseconds), reduced memory footprint (megabytes), and do not require feature engineering. Variations in the encoder and MLP architectures have been proposed to enhance APR accuracy. Furthermore, modifications to the loss function have been suggested to improve the balance between orientation and position objectives [16] or to incorporate other types of information [5]. For an in-depth examination of the various architectural designs and loss functions utilized in camera pose regression, please refer to [30].

2.2 Transformers

Originally developed for machine translation [38], Transformers have since become a state-of-the-art architecture in natural language processing. Recent studies have also shown the success of using Transformers to encode visual data [11]. Our work builds upon these studies by demonstrating the effectiveness of Transformers in incorporating the spatial information needed for accurate pose localization. In particular, to the best of our knowledge, we are the first to propose Transformer-Encoders as an efficient hypernetwork that adapts the weights of the regression heads based on the input query image.

2.3 Hypernetworks

Hypernetworks were first presented by Ha et al. [14]. These are neural networks that have been designed to predict the weights of a primary network. The primary network’s weights can be adjusted based on specific inputs, resulting in a more expressive and adaptive model. Hypernetworks have been used in various applications such as learning implicit neural representations [9], semantic segmentation [23], 3D scene representation and modeling [19, 33, 34] and continuous learning [39], to name a few.

3 Camera Pose Localization using Attention Hypernetworks

The proposed localization network consists of two main parts: the main network (APR), which is designed to estimate the camera’s absolute position, and the hypernetwork, which predicts the regression weights of the main network based on the input query image. The overall network is illustrated in Fig. 2 where the APR performs a forward pass on the input image to localize the capture camera. The camera pose is represented as the tuple $\langle \mathbf{x}, \mathbf{q} \rangle$, where $\mathbf{x} \in \mathbb{R}^3$ is the camera’s position in world coordinates and $\mathbf{q} \in \mathbb{R}^4$ is the quaternion encoding of its 3D orientation. Our method utilizes separate positional and orientational Transformer-Encoders to effectively integrate the flattened intermediate activation maps generated by a convolutional backbone. Following [8], we formulate the hypernetwork H as a parametric function $\theta_x = H(\theta, \mathbf{x})$, where θ represents the parameters of the hypernetwork,

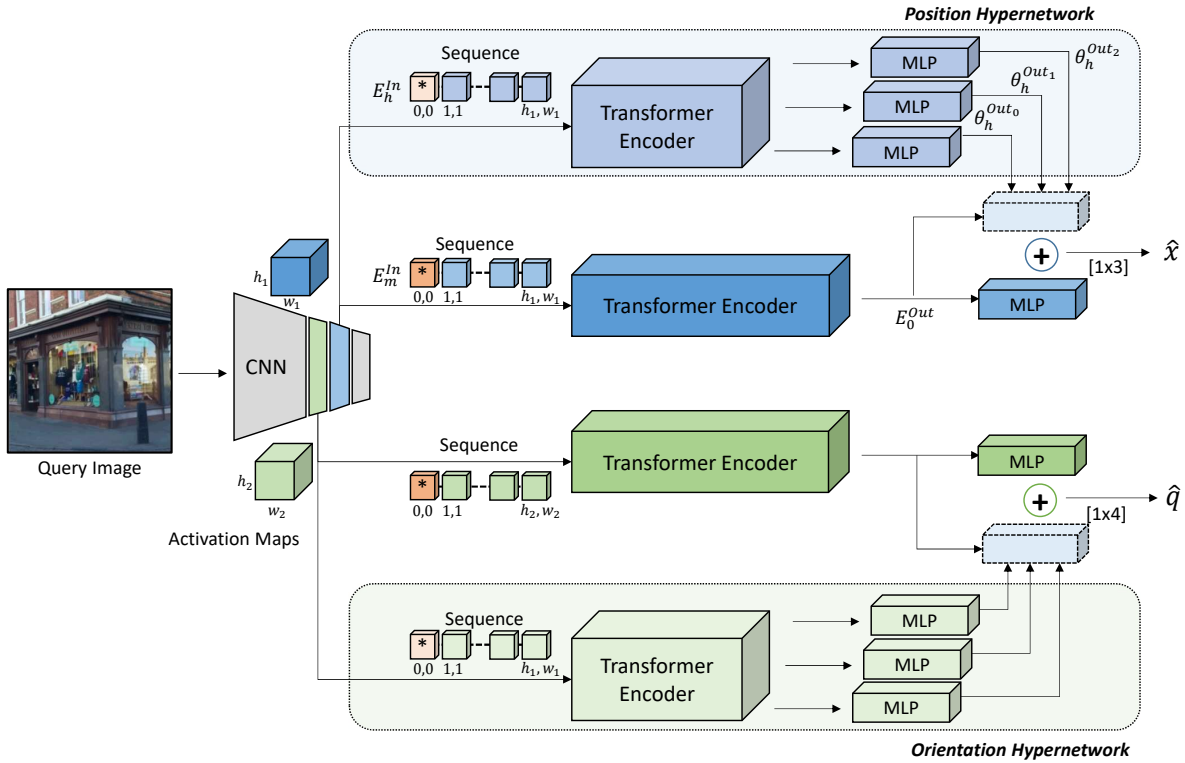


Figure 2: The proposed method consists of a dual-branch structure in the main network and an accompanying hypernetwork. The Transformer-Encoders in the main network sample activation maps generated by the convolutional backbone. In parallel, the hypernetwork generates a set of weights for the regression head of the main network, based on the input query image. The resulting adaptive weights, combined with the generalized latent vectors produced by each encoder in the main network, are utilized to estimate the camera pose components, either position (\hat{x}) or orientation (\hat{q}).

\mathbf{x} the input activation maps, and θ_x the parameters of the regression heads layer for the image \mathbf{x} .

3.1 Network Architecture

In line with Fig. 2, the input query image I_q is processed by a convolutional backbone that calculates the intermediate activation maps of two different layers. These activation maps are then utilized as inputs by both the main network’s and hypernetwork’s Transformer-Encoders. The hypernetwork’s encoders convert the activation maps into latent vectors through their processing. These latent vectors are then passed through multilayer perceptrons (MLPs) to generate the weights for the translation and orientation regression heads. Simultaneously, the positional and orientational encoders within the main network process the activation maps and integrate sequential representations into single latent vectors. These latent vectors are used to estimate camera position and orientation, using the weights θ_x generated by the hypernetwork H .

3.1.1 Main Network

The main network in the HyperPose architecture is composed of a convolutional backbone and two separate branches for regressing the camera’s position and orientation. Each branch includes its own Transformer-Encoder and a multilayer perceptron (MLP) head. Studies have demonstrated that substituting the patchify stem, utilized in early visual processing of a Vision Transformer (ViT), with a conventional convolutional stem enhances optimization stability and elevates peak performance to a higher level [43]. Hence, given an input query image $I_q \in \mathbb{R}^{H_q \times W_q \times C_q}$, a shared convolutional backbone generates activation maps. Two different activation maps are selected from the CNN based on the particular learned task. The activation maps, represented as $M \in \mathbb{R}^{H_M \times W_M \times C_M^{In}}$, are processed and transformed into $\tilde{M} \in \mathbb{R}^{H_M \times W_M \times C_M^{Out}}$ using a 1×1 convolutional layer, following the sequence preparation procedure described in [38]. To maintain the spatial relationships between the cells of the activation map, positional encoding is applied. The processed sequence is then augmented with a learned orientation/position token $T_m \in \mathbb{R}^{C_M^{Out}}$, creating a concatenated sequence that serves as the input to the task-

specific Transformer Encoder [10]:

$$E_m^{In} = [T_m, \tilde{M}] \in \mathbb{R}^{(H_M W_M=1) \times C_M^{Out}}. \quad (1)$$

The Transformer-Encoder consists of N blocks, all of which are identical in design. Each block is composed of a multi-head attention (MHA) mechanism for self-attention and a two-layer MLP with Swish activation functions [26] as specified in [7]. The input is subjected to Layer Normalization (LN) prior to processing by the MHA and MLP modules, as per [38]. The outputs of the MHA and MLP are then combined with the input via residual connections and dropout, following the approach outlined in [32]. As described in [11], position encoding is added to the input before each layer, and the final output undergoes additional LN normalization. The output at the position of the special token $E_{m_0}^{Out} \in \mathbb{R}^{C_M^{Out}}$, represents a context-aware and global summarization of the local features in the input activation map. Finally, based on the MLP weights output by the hypernetwork, the estimated camera position and orientation is regressed using the global summarized latent vector E_0^{Out} .

3.1.2 Hypernetwork

The hypernetwork, similar in design to the main network, consists of two distinct branches, each responsible for the regression of the weights for the regression position and orientation heads in the main network. Through the application of an identical preprocessing flow, a sequence is generated for the input of the Transformers encoders in the hypernetwork, derived from the encoded activation maps and learned tokens $T_h \in \mathbb{R}^{C_M^{Out}}$ [10]:

$$E_h^{In} = [T_h, \tilde{M}] \in \mathbb{R}^{(H_M W_M=1) \times C_M^{Out}}. \quad (2)$$

The global summarized latent vector from the encoders, $E_{h_0}^{Out} \in \mathbb{R}^{C_M^{Out}}$, is processed by multiple multilayer perceptrons (MLPs) followed by Swish activation functions, each of which is tasked with estimating the weights of a single corresponding layer in the regression heads of the main network:

$$\theta_h^{Out_i} = H(\theta_h^{Out_i}, E_{h_0}^{Out}) \in \mathbb{R}^{C_M^{Out} \times C_H^{Out_i}}, \quad (3)$$

where i is the index of the regression head layer.

3.2 Optimization Criteria

The localization error is calculated by comparing the translation position and orientation of the ground truth pose $\mathbf{p}_{gt} = \langle \mathbf{x}_{gt}, \mathbf{q}_{gt} \rangle$, where $\mathbf{x} \in \mathbb{R}^3$ represents the position of the camera in the world and $\mathbf{q} \in \mathbb{R}^4$ denotes its orientation encoded as a quaternion, with the estimated pose $\mathbf{p}_{est} = \langle \mathbf{x}_{est}, \mathbf{q}_{est} \rangle$. The translation error, represented by L_x , is commonly expressed in meters and is calculated as the Euclidean distance between the ground truth and the estimated camera positions. The orientation error, L_q , is defined as the Euclidean distance between the ground truth and the estimated unit vector quaternions [30]:

$$L_x = \|\mathbf{x}_0 - \mathbf{x}\|_2, \quad (4)$$

$$L_q = \left\| \mathbf{q}_0 - \frac{\mathbf{q}}{\|\mathbf{q}\|} \right\|_2 \quad (5)$$

where \mathbf{q} is a normalized norm quaternion to ensure it is a valid orientation encoding.

As a multi-regression optimization problem, we adopt the method outlined in [16] by using different weighting schemes, based on the uncertainty of each task, to balance the individual loss functions defined for the separate objectives. The model optimizes the aggregated loss function, which is a combination of the weighted individual losses.

$$L_p = L_x \exp(-s_x) + s_x + L_q \exp(-s_q) + s_q, \quad (6)$$

where s_x and s_q are the learned parameters. As a further optimization, we adopt the approach detailed in [31] and follow a three-step training process. Firstly, the entire network is trained using the aggregated loss described in Eq. 6. In the subsequent two steps, each MLP head is fine-tuned independently using its specific loss.

3.3 Implementation Details

In our shared convolutional backbone architecture, we employed an EfficientNet-B0 [36]. This model outperforms the accuracy of most existing convolutional neural networks and boasts improved efficiency. It consists of multiple levels of reduction, each representing activation maps with a reduced spatial resolution and an increased network depth. We used the activation maps of

two endpoints (reduction levels) as input for our position and orientation branches: $m_{rdct4} \in \mathbb{R}^{14 \times 14 \times 112}$ and $m_{rdct3} \in \mathbb{R}^{28 \times 28 \times 40}$, respectively. According to the method described in [32], we applied linear projections on each activation map to a common depth dimension of $C_M^{Out} = 256$ and learned the positional encoding of the same depth. Our implementation of the EfficientNet model is based on an open-source version [20]. In both the main network and the hypernetwork, we incorporated six-layer Transformer Encoders in each branch (position and orientation). Each block consists of a MHA layer with four heads, followed by an MLP that preserves the input dimension. A dropout rate of $p = 0.1$ was applied to each MLP layer. The output dimension of the Transformer-Encoders in the main network was set to $C_M^{Out} = 256$, while in the hypernetwork it was increased to $C_H^{Out} = 512$. The position and orientation branches of the hypernetwork generate the weights of three regression layers: input, hidden, and output. The number of weights in the position and orientation branches differ. The hypernetwork’s position branch produces the weights for an MLP with dimensions 512, 256, and 3, while the orientation branch generates weights for an MLP with dimensions 512, 512, and 4. The weights generated by the hypernetwork are then incorporated into the regression heads of the main network to estimate the position and orientation of the input query image. The input and hidden layers of the regression head utilize the Swish activation function.

4 Experimental Results

4.1 Datasets

The experimental evaluation was conducted using the 7 Scenes [13] and Cambridge Landmarks [17] APR evaluation benchmark datasets. The Cambridge Landmarks dataset represents an urban outdoor environment with a spatial extent ranging from approximately 900 to 5500 square meters. We present results for four of its six scenes, as the remaining two scenes have limited coverage in the existing literature or are reported to have possible faults. The 7 Scenes dataset consists of seven small-scale indoor scenes with a spatial extent ranging from approximately 1 to 10 square meters. These datasets present

various challenges commonly encountered in visual localization applications, including differences in scale, indoor/outdoor environments, repetitive elements, textureless features, significant viewpoint changes, and differences in trajectory between training and test sets.

4.2 Training Details

The training of the network is executed in three phases. During the first phase, all network components are trained simultaneously. In the second phase, only the translation-related layers, such as the hypernetwork and regression layers, are fine-tuned while other parts of the network are kept frozen. In the final phase, the orientation-related components are fine-tuned to achieve improved performance without compromising the localization objectives. The Adam optimization algorithm is used to minimize the loss function with $\beta_1 = 0.9$, $\beta_2 = 0.999$, and $\epsilon = 10^{-10}$ as the hyperparameters. The initial values of the loss parameters are established based on the characteristics of the dataset utilized. The batch size is set to 8, and the initial learning rate is $\lambda = 10^{-4}$. The learning rate decreases by 25% every 100 epochs for indoor localization and every 200 epochs for outdoor localization, with a maximum of 300 and 1000 epochs, respectively. Additionally, a weight decay of 10^{-4} and a dropout of $p = 0.1$ are applied to the encoders during training. Our model is subjected to augmentation procedures to enhance its generalization, in line with the approach used in [17]. During training, the image is resized so that its smaller edge is resized to 256 pixels and a random 224×224 crop is taken. Random adjustments are made to the brightness, contrast, and saturation of the image. During testing, the image is rescaled with the smaller edge resized to 256 pixels, and a center crop is taken without any further augmentation. The models were trained on multiple NVIDIA 2080Ti GPUs and the PyTorch framework.

4.3 Results

The primary objective of the proposed scheme is to improve the accuracy of absolute pose regression. To evaluate its performance, Tables 1 and 2 compare the median position error, measured in meters, and the orientation error, measured in degrees, of the proposed method with recent state-of-the-art localization algorithms on the

Cambridge Landmarks and 7 Scenes datasets, respectively. For both indoor and outdoor datasets, in addition to the results of leading APRs, we report the median position and orientation errors of structure-based, sequence-based, IR and RPR methods. Although DSAC [4] provides SOTA accuracy, our proposed method outperforms all other APRs methods. HyperPose achieves the lowest position estimation error in all scenes in both the Cambridge outdoor dataset and the 7Scenes indoor dataset, with the most accurate overall average of $0.87m$ and $0.17m$, respectively. Furthermore, HyperPose demonstrates the best orientational estimation error on both the Hospital and ShopFace scenes, in the Cambridge dataset.

4.4 Hypernetwork Output Weights

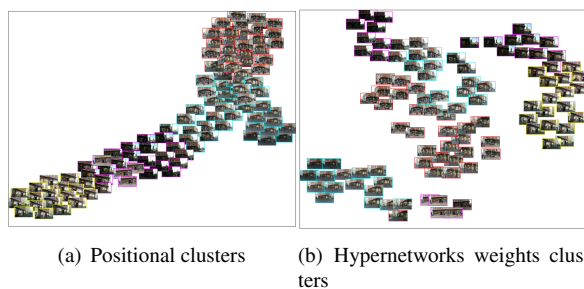


Figure 3: Clusters of the Shop Facade test set images, that are part of the Cambridge Landmarks dataset. The clusters are computed using K-Means with $K = 4$. (a) Clustering the corresponding camera (X, Y) positions. (b) Clustering the 2D t-SNE projections of the regression weights computed by the hypernetwork.

Given an input query image I_q , hypernetworks generate weights for the position and orientation regression heads, enabling adaptation of the network’s output based on the visual features present in the image. The scene depicted in the image is likely to exhibit a range of attributes, such as varying illumination conditions, different viewpoints, dynamic objects, and changing backgrounds. As a result, it is expected that the generated weights will be adapted to accommodate these fluctuations, so that the images from the same scene (location) will be jointly clustered despite the appearance variations, as shown in Fig. 3. Figure

Table 1: **Comparison to state-of-the-art methods: Cambridge Landmarks.** We report the median position/orientation error in meters/degrees for each method. The first and second most effective APRs are distinguished using **Red** and **Blue** colors, respectively.

		College	Hospital	Shop Facade	St. Mary	Avg.
Seq.	DSAC [4]	0.18,0.3°	0.21,0.4°	0.05,0.3°	0.15,0.5°	0.15,0.4°
	MapNet [5]	1.08,1.9°	1.94,3.9°	1.49,4.2°	2.00,4.5°	1.63,3.6°
	GL-Net [46]	0.59,0.7°	1.88,2.8°	0.50,2.9°	1.90,3.3°	1.22,2.4°
IR	VLAD [37]	2.80,5.7°	4.01,7.1°	1.11,7.6°	2.31,8.0°	2.56,7.1°
	VLAD+Inter [29]	1.48,4.5°	2.68,4.6°	0.90,4.3°	1.62,6.1°	1.67,4.9°
RPR	EssNet [47]	0.76,1.9°	1.39,2.8°	0.84,4.3°	1.32,4.7°	1.08,3.4°
	NC-EssNet [47]	0.61,1.6°	0.95,2.7°	0.7,3.4°	1.12,3.6°	0.85,2.8°
	RelocGNN[4]	0.48,1.0°	1.14,2.5°	0.48,2.5°	1.52,3.2°	0.91,2.3°
APR	PoseNet [17]	1.92,5.40°	2.31,5.38°	1.46,8.08°	2.65,8.48°	2.08,6.83° ²
	BayesianPN [15]	1.74,4.06°	2.57,5.14°	1.25,7.54°	2.11,8.38°	1.91,6.28°
	LSTM-PN [40]	0.99,3.65°	1.51,4.29°	1.18,7.44°	1.52,6.68°	1.30,5.57°
	SVS-Pose [22]	1.06,2.81°	1.50,4.03°	0.63,5.73°	2.11,8.11°	1.32,5.17°
	GPoseNet [6]	1.61,2.29°	2.62,3.89°	1.14,5.73°	2.93,6.46°	2.07,4.59°
	PoseNetLearn [16]	0.99,1.06°	2.17,2.94°	1.05,3.97°	1.49,3.43°	1.42,2.85°
	GeoPoseNet [16]	0.88,1.04°	3.20,3.29°	0.88,3.78°	1.57,3.32°	1.63,2.86°
	MapNet [5]	1.07,1.89°	1.94,3.91°	1.49,4.22°	2.00,4.53°	1.62,3.64°
	IRPNet [31]	1.18,2.19°	1.87,3.38°	0.72,3.47°	1.87,4.94°	1.41,3.50°
	MS-Trans-1S[32]	0.72,2.55°	2.07,3.24°	0.68,3.66°	1.10,5.26°	1.14,3.68°
	HyperPose (Ours)	0.56,2.40°	1.41,2.91°	0.54,3.37°	0.98,4.86°	0.87,3.43°

3(a) depicts the clustering of the Shop Facade scene test set from the Cambridge Landmarks dataset. The spatial (X,Y) coordinates were clustered using K-Means with $K = 4$. The images are colored according to their cluster index. As expected, the clusters were formed based on the proximity and location of the images within the scene’s coordinates. Figure 2(b) shows the K-Means clustering of the 2D t-SNE projections of the regression weights generated by the hypernetwork. Figure 3(b) shows that the images are grouped based on their visual attributes and viewing angles, which demonstrates that the hypernetwork adapts its output to the input image. This differs from other state-of-the-art APR solutions, where the regression head weights are static and learned during the training phase, thus restricting their ability to adapt to the variations in input images.

4.5 Ablation Study

In order to gauge the performance of the chosen architecture, we performed an ablation study. The comparison was based on the model’s performance on the ShopFacade scene in the Cambridge Landmarks dataset, measured at the end of the initial training phase. For each ablation, we changed and studied a single scheme parameter.

Residual hypernetwork output. Table 3 presents the results obtained by regressing both the absolute pose and the residual additive branch, to support the reasoning behind the configuration of the hypernetworks to output the residual position and orientation. The residual-based architecture outperforms the direct regression approach, as evidenced by the lower errors in both position and orientation estimation achieved by the former.

Hypernetwork embedding dimension. We assess the

Table 2: **Comparison with state-of-the-art methods: 7Scenes.** We report the median position/orientation error in meters/degrees for each method. The first and second most effective APRs are distinguished using **Red** and **Blue** colors, respectively.

		Chess	Fire	Heads	Office	Pumpkin	Kitchen	Stairs
Seq.	DSAC* [4]	0.02,1.1°	0.02,1.0°	0.01,1.8°	0.03,1.2°	0.04,1.4°	0.03,1.7°	0.04,1.4°
	LsG [45]	0.09,3.3°	0.26,10.9°	0.17,12.7°	0.18,5.5°	0.20,3.7°	0.23,4.9°	0.23,11.3°
	MapNet[5]	0.08,3.3°	0.27,11.7°	0.18,13.3°	0.17,5.2°	0.22,4.0°	0.23,4.9°	0.30,12.1°
	GL-Net[46]	0.08,2.8°	0.26,8.9°	0.17,11.4°	0.18,13.3°	0.15,2.8°	0.25,4.5°	0.23,8.8°
IR	VLAD [37]	0.21,12.5°	0.33,13.8°	0.15,14.9°	0.28,11.2°	0.31,11.2°	0.30,11.3°	0.25,12.3°
	VLAD+Inter[29]	0.18,10.0°	0.33,12.4°	0.14,14.3°	0.25,10.1°	0.26,9.4°	0.27,11.1°	0.24,14.7°
RPR	NN-Net [18]	0.13,6.5°	0.26,12.7°	0.14,12.3°	0.21,7.4°	0.24,6.4°	0.24,8.0°	0.27,11.8°
	RelocNet[1]	0.12,4.1°	0.26,10.4°	0.14,10.5°	0.18,5.3°	0.26,4.2°	0.23,5.1°	0.28,7.5°
	EssNet [47]	0.13,5.1°	0.27,10.1°	0.15,9.9°	0.21,6.9°	0.22,6.1°	0.23,6.9°	0.32,11.2°
	NC-EssNet [47]	0.12,5.6°	0.26,9.6°	0.14,10.7°	0.20,6.7°	0.22,5.7°	0.22,6.3°	0.31,7.9°
	RelocGNN[4]	0.08,2.7°	0.21,7.5°	0.13,8.70°	0.15,4.1°	0.15,3.5°	0.19,3.7°	0.22,6.5°
APR	PoseNet [17]	0.32,8.12°	0.47,14.4°	0.29,12.0°	0.48,7.68°	0.47,8.42°	0.59,8.64°	0.47,13.8°
	BayesianPN [15]	0.37,7.24°	0.43,13.7°	0.31,12.0°	0.48,8.04°	0.61,7.08°	0.58,7.54°	0.48,13.1°
	LSTM-PN [40]	0.24,5.77°	0.34,11.9°	0.21,13.7°	0.30,8.08°	0.33,7.00°	0.37,8.83°	0.40,13.7°
	GPoseNet [6]	0.20,7.11°	0.38,12.3°	0.21,13.8°	0.28,8.83°	0.37,6.94°	0.35,8.15°	0.37,12.5°
	PoseNetLearn[16]	0.14,4.50°	0.27,11.8°	0.18,12.1°	0.20,5.77°	0.25,4.82°	0.24,5.52°	0.37,10.6°
	GeoPoseNet[16]	0.13,4.48°	0.27,11.3°	0.17,13.0°	0.19,5.55°	0.26,4.75°	0.23,5.35°	0.35,12.4°
	MapNet[5]	0.08,3.25°	0.27,11.7°	0.18,13.3°	0.17,5.15°	0.22,4.02°	0.23,4.93°	0.30,12.1°
	IRPNet[31]	0.13,5.64°	0.25,9.67°	0.15,13.1°	0.24,6.33°	0.22,5.78°	0.30,7.29°	0.34,11.6°
	AttLoc[41]	0.10,4.07°	0.25,11.4°	0.16,11.8°	0.17,5.34°	0.21,4.37°	0.23,5.42°	0.26,10.5°
	MS-Trans-1S[32]	0.10,5.86°	0.23,11.0°	0.15,12.8°	0.17,6.56°	0.18,5.32°	0.17,6.30°	0.26,11.3°
	HyperPose (Ours)	0.08,6.29°	0.22,11.2°	0.11,12.7°	0.17,7.53°	0.16,6.66°	0.17, 8.48°	0.26,10.8°

Table 3: Ablation study of the network residual architecture. We report the median position and orientation errors.

Architecture	Position [meters]	Orientation [degrees]
Direct Regression	0.55	4.06
Residual Regression	0.53	3.55

effect of altering the size of the fully-connected layers in both the position and orientation branches of the regression heads. The results of our experiment are shown in

Table 4, where we present the results obtained by varying the dimensions of the layers.

Hypernetwork architecture. We evaluated using an alternative conventional MLP-based hypernetwork design. This design computes the regression layer weights using an MLP, whose input is the terminal latent vector of the EfficientNet-B0 backbone. The proposed attention-hypernetwork architecture exhibits superior performance in estimating both positional and orientational errors. A plausible explanation is that spatial information is already condensed into a vector by the output of the backbone network, which constrains the MLP-based hypernetwork branches from addressing finer details in the activation

Table 4: Ablation study of the embedding dimension regressed by the hypernetworks. We report the median position and orientation errors.

Embedding Dimensions [Position/Orientation]	Position [meters]	Orientation [degrees]
256/256	0.66	4.3
256/512	0.53	3.55
512/512	0.68	4.33

maps.

Table 5: Ablations hypernetwork architecture. We report the median position and orientation errors.

Architecture	Position [meters]	Orientation [degrees]
Backbone embedding	0.68	4.29
Transformer-Encoders	0.57	4.06

Hypernetwork output layers. By design, the output of hypernetworks determines the number of regression layers in the regression heads of the main network. Table 6 details the position estimation error vs. the number of layers.

Table 6: Ablations of the hypernetwork number of output weights. We report the median position and orientation errors.

Regressed Layers	Position [meters]	Orientation [degrees]
Single Layer	0.64	4.13
Input/Output layers	0.65	3.99
Input/Hidden/Output layers	0.66	3.55

Rotation representations. The authors of [48] contend that 3D and 4D rotation representations are suboptimal for network regression, whereas continuous representations in 5D and 6D are more appropriate for learning.

As shown in Table 7, employing a 4D-based representation in conjunction with the rotational loss specified in Eq. 5 led to the lowest orientational estimation error. In both the Quaternions and 4D-Norm approaches, the rotation regressor generates four values that estimate the camera’s orientation (quaternion), but the latter computes the orientation loss based on rotation matrices instead.

Table 7: Ablation of the 3D rotation encoding. We report the median orientation errors.

Rotation representation	Orientation [degrees]
Quaternions	3.55
4D-Norm [48]	4.08
6D [48]	4.54

5 Conclusions

In this study, we present a novel attention-based architecture for absolute pose regression that uses a hypernetwork to estimate the regression head weights. This allows us to improve localization accuracy by adapting the regression weights to the input image embedding. To the best of our knowledge, this is the first use of hypernetworks to have been used in localization in general, and the first use of Transformer-Encoders in hypernetworks, in particular. Our approach is shown to compare favorably with contemporary APR schemes.

References

- [1] Vassileios Balntas, Shuda Li, and Victor Prisacariu. Relocnet: Continuous metric learning relocalisation using neural nets. In *Proceedings of the European Conference on Computer Vision (ECCV)*, September 2018. 9
- [2] E. Brachmann, A. Krull, S. Nowozin, J. Shotton, F. Michel, S. Gumhold, and C. Rother. DSAC - differentiable RANSAC for camera localization. In *Proceedings of the IEEE/CVF Conference on Computer Vision and Pattern Recognition (CVPR)*, pages 2492–2500, Los Alamitos, CA, USA, jul 2017. 1, 3

- [3] E. Brachmann and C. Rother. Learning less is more - 6D camera localization via 3D surface regression. In *Proceedings of the IEEE/CVF Conference on Computer Vision and Pattern Recognition (CVPR)*, pages 4654–4662, 2018. 1, 3
- [4] E. Brachmann and C. Rother. Visual camera relocalization from rgb and rgb-d images using dsac. *IEEE Transactions on Pattern Analysis and Machine Intelligence*, (01):1–1, apr 2021. 3, 7, 8, 9
- [5] Samarth Brahmabhatt, Jinwei Gu, Kihwan Kim, James Hays, and Jan Kautz. Geometry-aware learning of maps for camera localization. In *Proceedings of the IEEE/CVF Conference on Computer Vision and Pattern Recognition (CVPR)*, 2018. 3, 8, 9
- [6] Ming Cai, Chunhua Shen, and Ian Reid. A hybrid probabilistic model for camera relocalization. In *Proceedings of the British Machine Vision Conference*, page 238, 2018. 1, 2, 8, 9
- [7] Nicolas Carion, Francisco Massa, Gabriel Synnaeve, Nicolas Usunier, Alexander Kirillov, and Sergey Zagoruyko. End-to-end object detection with transformers. In *Proceedings of the European Conference on Computer Vision (ECCV)*, pages 213–229, Cham, 2020. 5
- [8] Yoav Chai, Raja Giryes, and Lior Wolf. Supervised and unsupervised learning of parameterized color enhancement. In *Proceedings of the IEEE/CVF Winter Conference on Applications of Computer Vision (WACV)*, pages 992–1000, 2020. 3
- [9] Yinbo Chen and Xiaolong Wang. Transformers as meta-learners for implicit neural representations. In *Proceedings of the European Conference on Computer Vision (ECCV)*, pages 170–187. Springer, 2022. 2, 3
- [10] Alexey Dosovitskiy, Lucas Beyer, Alexander Kolesnikov, Dirk Weissenborn, Xiaohua Zhai, Thomas Unterthiner, Mostafa Dehghani, Matthias Minderer, Georg Heigold, Sylvain Gelly, et al. An image is worth 16x16 words: Transformers for image recognition at scale. *arXiv preprint arXiv:2010.11929*, 2020. 5
- [11] Alexey Dosovitskiy, Lucas Beyer, Alexander Kolesnikov, Dirk Weissenborn, Xiaohua Zhai, Thomas Unterthiner, Mostafa Dehghani, Matthias Minderer, Georg Heigold, Sylvain Gelly, Jakob Uszkoreit, and Neil Houlsby. An image is worth 16x16 words: Transformers for image recognition at scale. In *Proceedings of the International Conference on Learning Representations (ICLR)*, 2021. 3, 5
- [12] M. Dusmanu, I. Rocco, T. Pajdla, M. Pollefeys, J. Sivic, A. Torii, and T. Sattler. D2-net: A trainable cnn for joint description and detection of local features. In *Proceedings of the IEEE/CVF Conference on Computer Vision and Pattern Recognition (CVPR)*, pages 8084–8093, 2019. 2
- [13] B. Glocker, S. Izadi, J. Shotton, and A. Criminisi. Real-time rgb-d camera relocalization. In *2013 IEEE International Symposium on Mixed and Augmented Reality (ISMAR)*, pages 173–179, 2013. 6
- [14] David Ha, Andrew Dai, and Quoc V Le. Hypernetworks. *arXiv preprint arXiv:1609.09106*, 2016. 1, 3
- [15] Alex Kendall and Roberto Cipolla. Modelling uncertainty in deep learning for camera relocalization. In *Proceedings of the IEEE International Conference on Robotics and Automation (ICRA)*, pages 4762–4769, 2016. 1, 2, 8, 9
- [16] A. Kendall and R. Cipolla. Geometric loss functions for camera pose regression with deep learning. In *Proceedings of the IEEE/CVF Conference on Computer Vision and Pattern Recognition (CVPR)*, pages 6555–6564, 2017. 1, 3, 6, 8, 9
- [17] A. Kendall, M. Grimes, and R. Cipolla. Posenet: A convolutional network for real-time 6-dof camera relocalization. In *Proceedings of the IEEE International Conference on Computer Vision (ICCV)*, pages 2938–2946, 2015. 1, 2, 3, 6, 7, 8, 9
- [18] Z. Laskar, I. Melekhov, S. Kalia, and J. Kannala. Camera relocalization by computing pairwise relative poses using convolutional neural network. In *Proceedings of the IEEE International Conference on Computer Vision Workshops (ICCVW)*, pages 920–929, 2017. 9
- [19] Gidi Littwin and Lior Wolf. Deep meta functionals for shape representation. In *Proceedings of the IEEE International Conference on Computer Vision (ICCV)*, pages 1824–1833, 2019. 3
- [20] Luke Melaskyriazi. *efficientnet-pytorch*, 2019. 6
- [21] Iaroslav Melekhov, Juha Ylioinas, Juho Kannala, and Esa Rahtu. Image-based localization using hourglass networks. In *Proceedings of the IEEE International Conference on Computer Vision Workshops (ICCVW)*, pages 870–877, 2017. 1
- [22] Tayyab Naseer and W. Burgard. Deep regression for monocular camera-based 6-dof global localization in outdoor environments. *2017 IEEE/RSJ International Conference on Intelligent Robots and Systems (IROS)*, pages 1525–1530, 2017. 1, 8
- [23] Yuval Nirkin, Lior Wolf, and Tal Hassner. Hyperseg: Patch-wise hypernetwork for real-time semantic segmentation. In *Proceedings of the IEEE/CVF Conference on Computer Vision and Pattern Recognition (CVPR)*, pages 4061–4070, 2021. 2, 3
- [24] H. Noh, A. Araujo, J. Sim, T. Weyand, and B. Han. Large-scale image retrieval with attentive deep local features. In *Proceedings of the IEEE International Conference on Computer Vision (ICCV)*, pages 3476–3485, 2017. 2

- [25] N. Radwan, A. Valada, and W. Burgard. Vlocnet++: Deep multitask learning for semantic visual localization and odometry. *IEEE Robotics and Automation Letters*, 3(4):4407–4414, 2018. [2](#)
- [26] Prajit Ramachandran, Barret Zoph, and Quoc V Le. Searching for activation functions. *arXiv preprint arXiv:1710.05941*, 2017. [5](#)
- [27] P. Sarlin, C. Cadena, R. Siegwart, and M. Dymczyk. From coarse to fine: Robust hierarchical localization at large scale. In *Proceedings of the IEEE/CVF Conference on Computer Vision and Pattern Recognition (CVPR)*, pages 12708–12717, 2019. [1](#), [2](#)
- [28] T. Sattler, B. Leibe, and L. Kobbelt. Efficient effective prioritized matching for large-scale image-based localization. *IEEE Transactions on Pattern Analysis and Machine Intelligence*, 39(9):1744–1756, 2017. [1](#)
- [29] T. Sattler, Q. Zhou, M. Pollefeys, and L. Leal-Taixé. Understanding the limitations of cnn-based absolute camera pose regression. In *Proceedings of the IEEE/CVF Conference on Computer Vision and Pattern Recognition (CVPR)*, pages 3297–3307, 2019. [8](#), [9](#)
- [30] Yoli Shavit and Ron Ferens. Introduction to camera pose estimation with deep learning. In *arXiv preprint arXiv:1907.05272*, 2019. [1](#), [3](#), [6](#)
- [31] Yoli Shavit and Ron Ferens. Do we really need scene-specific pose encoders? In *Proceedings of the International Conference on Pattern Recognition (ICPR)*, pages 3186–3192. IEEE, 2021. [1](#), [2](#), [6](#), [8](#), [9](#)
- [32] Yoli Shavit, Ron Ferens, and Yosi Keller. Learning multi-scene absolute pose regression with transformers. In *Proceedings of the IEEE International Conference on Computer Vision (ICCV)*, 2021. [2](#), [5](#), [6](#), [8](#), [9](#)
- [33] Vincent Sitzmann, Julien Martel, Alexander Bergman, David Lindell, and Gordon Wetzstein. Implicit neural representations with periodic activation functions. *Advances in Neural Information Processing Systems (NIPS)*, 33:7462–7473, 2020. [3](#)
- [34] Przemysław Spurek, Artur Kasymov, Marcin Mazur, Diana Janik, Slawomir K Tadeja, J Tabor, T Trzciński, et al. Hyperpocket: Generative point cloud completion. In *2022 IEEE/RSJ International Conference on Intelligent Robots and Systems (IROS)*, pages 6848–6853. IEEE, 2022. [3](#)
- [35] H. Taira, M. Okutomi, T. Sattler, M. Cimpoi, M. Pollefeys, J. Sivic, T. Pajdla, and A. Torii. Inloc: Indoor visual localization with dense matching and view synthesis. *IEEE Transactions on Pattern Analysis and Machine Intelligence*, pages 1–1, 2019. [1](#)
- [36] Mingxing Tan and Quoc Le. EfficientNet: Rethinking model scaling for convolutional neural networks. volume 97 of *Proceedings of Machine Learning Research*, pages 6105–6114, Long Beach, California, USA, 09–15 Jun 2019. [6](#)
- [37] Akihiko Torii, Relja Arandjelovic, Josef Sivic, Masatoshi Okutomi, and Tomas Pajdla. 24/7 place recognition by view synthesis. In *Proceedings of the IEEE/CVF Conference on Computer Vision and Pattern Recognition (CVPR)*, 2015. [8](#), [9](#)
- [38] Ashish Vaswani, Noam Shazeer, Niki Parmar, Jakob Uszkoreit, Llion Jones, Aidan N Gomez, Łukasz Kaiser, and Illia Polosukhin. Attention is all you need. In *Advances in Neural Information Processing Systems (NIPS)*, volume 30, pages 5998–6008, 2017. [3](#), [5](#)
- [39] Johannes Von Oswald, Christian Henning, João Sacramento, and Benjamin F Grewe. Continual learning with hypernetworks. *arXiv preprint arXiv:1906.00695*, 2019. [3](#)
- [40] F. Walch, C. Hazirbas, L. Leal-Taixé, T. Sattler, S. Hilsenbeck, and D. Cremers. Image-based localization using lstms for structured feature correlation. In *Proceedings of the IEEE International Conference on Computer Vision (ICCV)*, pages 627–637, 2017. [1](#), [2](#), [8](#), [9](#)
- [41] Bing Wang, Changhao Chen, Chris Xiaoxuan Lu, Peijun Zhao, Niki Trigoni, and Andrew Markham. Atloc: Attention guided camera localization. In *Proceedings of the AAAI Conference on Artificial Intelligence*, volume 34, pages 10393–10401, 2020. [1](#), [9](#)
- [42] J. Wu, L. Ma, and X. Hu. Delving deeper into convolutional neural networks for camera relocalization. In *Proceedings of the IEEE International Conference on Robotics and Automation (ICRA)*, pages 5644–5651, 2017. [1](#)
- [43] Tete Xiao, Mannat Singh, Eric Mintun, Trevor Darrell, Piotr Dollár, and Ross Girshick. Early convolutions help transformers see better. *Advances in Neural Information Processing Systems (NIPS)*, 34:30392–30400, 2021. [5](#)
- [44] Meng Xu, Youchen Wang, Bin Xu, Jun Zhang, Jian Ren, Stefan Poslad, and Pengfei Xu. A critical analysis of image-based camera pose estimation techniques. *arXiv preprint arXiv:2201.05816*, 2022. [1](#)
- [45] Fei Xue, Xin Wang, Zike Yan, Qiuyuan Wang, Junqiu Wang, and Hongbin Zha. Local supports global: Deep camera relocalization with sequence enhancement. In *Proceedings of the IEEE/CVF Conference on Computer Vision and Pattern Recognition (CVPR)*, 2019. [9](#)
- [46] Fei Xue, Xin Wu, Shaojun Cai, and Junqiu Wang. Learning multi-view camera relocalization with graph neural networks. In *Proceedings of the IEEE/CVF Conference on Computer Vision and Pattern Recognition (CVPR)*, 2020. [8](#), [9](#)
- [47] Qunjie Zhou, Torsten Sattler, Marc Pollefeys, and Laura Leal-Taixé. To learn or not to learn: Visual localization

from essential matrices. In *Proceedings of the IEEE International Conference on Robotics and Automation (ICRA)*, pages 3319–3326. IEEE, 2020. [3](#), [8](#), [9](#)

- [48] Yi Zhou, Connelly Barnes, Jingwan Lu, Jimei Yang, and Hao Li. On the continuity of rotation representations in neural networks. In *Proceedings of the IEEE/CVF Conference on Computer Vision and Pattern Recognition (CVPR)*, pages 5745–5753, 2019. [10](#)